Computation of Near-Field and Far-Field Radiation Characteristics of Acoustic Transducers for Underwater Acoustic Imaging

Praveen L. S.[1], Govind R. Kadambi[2], S. Malathi[3], Preetham Shankapal[4]

Abstract – *This paper proposes a novel approach through analytical formulation for the determination of the radiation pattern of acoustic transducers at any arbitrary observation distance which covers both the near-field as well as the far-field. The proposed near-field/far-field analysis is generic and can be applied to a wide variety of acoustic apertures. The radiation pattern of the acoustic transducer at any arbitrary point of observation (both the near-field and far-field) is obtained by the vector summation of the fields radiated by the array of point sources located on the aperture of the acoustic transducer. The validity and novelty of the proposed approach have been proved by treating the far-field as a special case of near-field with relevant distance criterion. The simulation studies show that near-field radiation patterns of the acoustic transducer exhibit changes in the profile of the amplitude patterns when the distance of observation is varied. The formation of a well-defined main beam of the radiation pattern occurs only after a distance of separation of about $R=1.2D^2/\lambda$ from the radiating aperture. The presented analytical formulation has an attribute of wider generality in view of its applicability to a variety of geometrical configurations of the aperture of an acoustic transducer.*

Keywords: *Aperture, Far Field (FF), Near Field (NF), Radiation Pattern, Underwater Acoustic Imaging (UAI)*

I. Introduction

Underwater Acoustic Imaging (UAI) is the study of the propagation of sound waves in water. It provides underwater observation and inspection capabilities wherever optical systems cannot. In UAI, Sound Navigation and Ranging (SONAR) is used to detect and classify objects in underwater using acoustic waves. UAI is a cross-disciplinary domain which involves acoustic transducer, waveform design, beamforming, motion compensation, and image processing among others. UAI system is similar to other forms of acoustic imaging such as medical and non-destructive testing where it provides two-dimensional images of objects using sound waves. UAI is used for various applications like navigation, surveillance, reconnaissance and ranging. Some of the commercial applications of UAI comprise planning underwater communication links for discovering underwater mining resources. UAI finds utility in military applications such as locating submarines and mines. Modern applications of UAI involve developing autonomous underwater vehicles equipped with acoustic imaging devices to monitor and explore the seafloor. The operating frequency of underwater acoustics ranges from 10 Hz to 1 MHz [1]. Lower frequencies offer a longer range with poor resolution while higher frequencies facilitate better resolution but a shorter range. Hence for UAI systems, the operating frequency will be typically in the range of 10 kHz to 300 kHz with a bandwidth of 30 kHz and wavelength 0.005m to 0.15m [2]. SONAR is used for exploring and mapping the underwater scenario because sound wave travels long distances in the water compared to the light waves. There are many efficient approaches used in UAI like the Synthetic Aperture Sonar (SAS) and Inverse Synthetic Aperture Sonar (ISAS) [3]-[4]. But they both have their own merits and demerits in computing efficiency, hardware requirement and developing high-resolution images. SAS suffers from a slow mapping rate. The difficulty in maintaining phase coherence throughout the entire synthesized aperture results in significant image degradation [5]. Both SAS and ISAS imaging requires relative motion between the target and the radiating system. Without the above mentioned relative motion, the image does not form [6].

Both SAS and ISAS methods use different beamforming techniques to illuminate the targets in underwater using the acoustic transceiver. Beamforming is a signal processing technology used to control the directionality of signal transmission (or) reception. Beamforming has been in use for many years in the field of SONARs in which both amplitude and phase shift (weights) at each acoustic transducer are used to control the directionality of the transmitted or received beam as shown in Fig. 1.

Manuscript received and revised xx 2010, accepted xx 2010

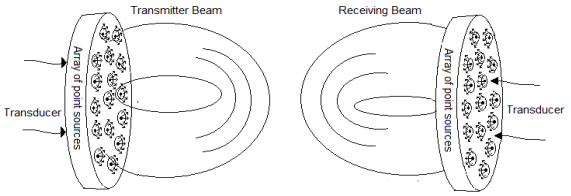

(a) (b)

Fig. 1. Array of point sources on acoustic transducer [7]

In far-field, the rays carrying acoustic field incident on different point sources located on the aperture of acoustic transducer are always parallel (Fig. 2(a)), whereas in the near-field beamforming, rays impinging on the acoustic aperture are not assumed to be parallel. The distance between the source of acoustic field and the receiver is small (Fig. 2(b)) [8]. Well established far-field methods for measuring radiation patterns of an acoustic transducer in the underwater scenario cannot be used in many cases due to the large aperture size of the acoustic transducers. The radiating far-field distance may be too long (or) impractical to move the acoustic transducer from its operating environment to the desired range. Radiating acoustic power (pressure) decreases as the square of the distance from the transmitter resulting in poor image quality. For a given observation point, the near field beamforming array exhibits differing radiation patterns in terms of both amplitude and phase. Therefore the computation of near-field radiation patterns of the acoustic transducer which forms an element of a beamforming array becomes an important step in simulation near-field beamforming.

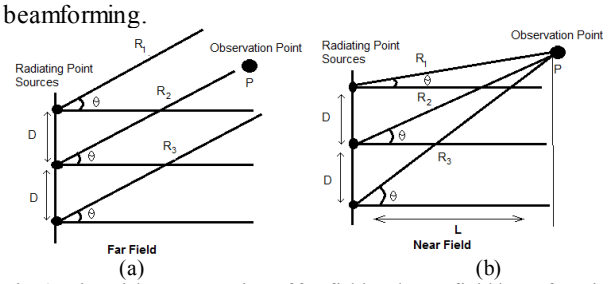

(a) (b)

Fig. 2. Pictorial representation of far-field and near-field beamforming [8]

Selfridge (1980) [9] discusses the analysis of the far-field radiation pattern of narrow-strip acoustic transducer for underwater imaging. Rongrong (2014) [10] illustrates the measurement of far-field radiation patterns for dipole acoustic transducers. Hayden (2003) [11] describes the mathematical modeling of the SAS system, offering improved Fourier based image reconstruction by analyzing the far-field beamformer for seafloor detection. Stepanishen (2005) [12] has presented a computation method for the far-field radiation pattern from cylindrical pistons. The author has also described a method for computing the interacting forces and mutual radiation impedance. There is an abundance of literature on the far-field techniques of UAI. However, the reported research on near–field analysis of UAI appears to be rather limited in the open literature. From the literature, it is observed that for far-field radiation pattern of the acoustic transducer, each of the analysis had been specifically developed by keeping the geometric configuration of the acoustic aperture. Also, they cannot be extended to treat near-field analysis or to other geometric configurations of acoustic aperture. This paper proposes a novel technique which is valid for computing the radiation pattern at any arbitrary distance (near-field and far-field) from the transducer. The presented analytical formulation has an attribute of wider generality given its applicability to a variety of geometrical configurations of the aperture of the acoustic transducer.

II. Analytical Formulation for Near Field Radiation Pattern of Acoustic Transducer

This section presents a generalized procedure for computing the near-field radiation pattern of an acoustic transducer. The method of determination of the near-field radiation pattern invokes the concepts of equivalent pressure distribution *"p"* from an acoustic source and the field radiated by the point sources located on the aperture of the acoustic transducer. In the proposed method, the radiating aperture of an acoustic transducer is replaced by an array of point sources whose pressure strength is determined by the field distribution at the respective locations of point sources on the acoustic transducer [13]. The proposed method is versatile and generic which applies to any geometric configuration provided that the field distribution of acoustic transducer is known. This paper considers the circular and rectangular apertures for the analysis of field distribution. The circular and rectangular apertures associated with Cartesian coordinate points for the analysis of the near-field radiation pattern are shown in Fig. 3.

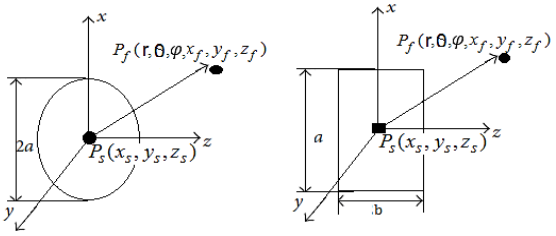

(a) (b)

Fig. 3. Coordinate system of circular and rectangular aperture for near-field analysis

The radiating aperture of the circular and rectangular acoustic transducer is assumed to coincide with "$Z = 0$"plane and the observation point of interest "P" is in the near-field range from the transducer. The diameter of a circular aperture is $d = 2r$ where, "r" is radius of an aperture. For the rectangular aperture $L \times H = a \times b$ is as shown in Fig. 3. The criterion for the definition of far-field distance "R" is $R \geq 2D^2/\lambda$, where D is the dimension of the transducer and "λ" is the wavelength. Any distance of observation with "R", $R < 2D^2/\lambda$ is termed as near field. The near-field in turn is divided into two more regions as stated in [14]:

a. Reactive near-field: $R < 0.62\sqrt{D^3/\lambda}$
b. Radiating near-field: $0.62\sqrt{D^3/\lambda} < R < 2D^2/\lambda$.

The computation of near-field radiation pattern from acoustic transducer to the observation point is carried out with $0.62\sqrt{D^3/\lambda} < R < 2D^2/\lambda$. The region greater or equal to the distance $2D^2/\lambda$ is referred as far-field region ($R \geq 2D^2/\lambda$). In this region normalized radiation pattern is basically independent of the distance from the acoustic transducer [15]. This paper proposes a generic method that is valid to compute the radiation pattern of the acoustic transducer with the observation points lying in either near-field or far-field region.

II.1. *Pressure Distribution at Various Point Sources on Acoustic Aperture*

The radiating surface (aperture) of the acoustic transducer is considered to be comprised of several miniature sized point sources (elements). Each of the point sources has an area of "*ds*" as shown in Fig. 4. Each point source with a diameter much smaller than the wavelength of operation transmits spherical waves in all directions [16].

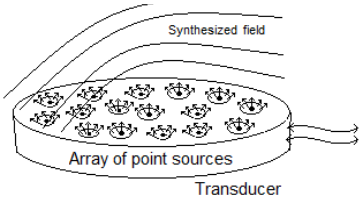

Fig. 4. Field distribution from an array of point sources

Wave propagation from a point source is illustrated in Fig. 5. Where "r_0" is the radius of the simple source; "P_0" denotes the pressure at the surface, and the pressure at a radial distance "r" is denoted as "P_r".

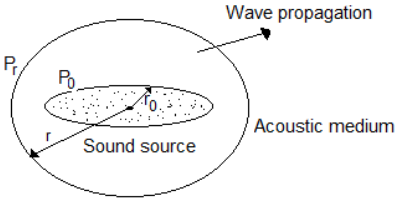

Fig. 5. A point source transmitting a spherical wave with reference pressure P_0 at a reference distance r_0

The point source emits spherical waves of radiation in an ideal uniform medium. In point source the pulsating sphere diameter is smaller than the wavelength of the radiated waves. The radiating waves are spread uniformly over a complete spherical surface at any radius from source. The pressure "P_r" is inversely proportional to radius "r" and hence the pressure amplitude of the wave decreases as their distance from the point source increases [13]. Hence, the far field radiation pattern of a point source is given by:

$$P_m(r) = A_m \cdot \frac{e^{-jk_m r_m}}{r_m} ds \quad (1)$$

Where, "$P_m(r)$" is the corresponding field of point sources at distance "r_m". The constant "A_m" defines the reference amplitude at the reference distance "r_m", "k_m" is the wave number and $j=\sqrt{(-1)}$ [17]. The velocity of the acoustic source "V_m" at a point z due to the m^{th} point source is demonstrated in Fig. 6. The characteristics of the radiation pattern of acoustic aperture are significantly determined by the size and shape of the radiating element, propagation mode, and the distance of the radiating element to the observation point and the frequency of operation. The most commonly used radiating aperture in acoustic engineering is either rectangular or circular. The following section discusses the computation of the radiation pattern of circular and rectangular apertures.

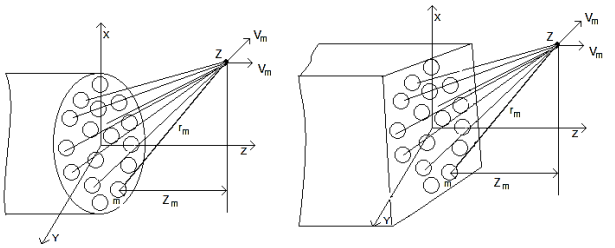

Fig. 6. Field distribution at observation point z with velocity V_m from m^{th} point source

II.2. *Computation of Radiation Pattern of Circular Acoustic Aperture*

The Cartesian coordinates of point sources on circular aperture at a distance "R" for computing the radiation pattern are shown in Fig. 7. The circular radiating aperture consists of a number of point sources with dimension "ds" at distance "ρ" from the center of the aperture. Each point source generates spherical waves in all directions with the pressure field "P_S".

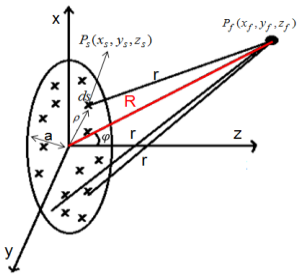

Fig. 7. Coordinate system of circular aperture for analysis radiation pattern

The pressure field distribution at an observation point $P_f(x_f, y_f, z_f)$ from point sources $P_s(x_s, y_s, z_s)$ located on circular aperture at distance "r" from the center of aperture is given by:

$$P_f(x_f, y_f, z_f) = \iint_{surface}^{a} P_s ds$$

$$P_f(x_f, y_f, z_f) = A_0 \int_{\rho=0}^{a} \int_{\varphi=0}^{2\pi} \frac{e^{-jkr}}{r} \rho \, d\rho \, d\varphi \quad (2)$$

Where, $\rho = 0\ to\ a$
$\varphi = 0\ to\ 2\pi$

In Eq. 2, "P_s" indicates the pressure field at a point source on the acoustic aperture, "a" is radius of circular aperture, "r" is distance from the observation point "P_f" to the point source "P_s", "R" is the range or distance between the observation point and the center of circular aperture, and "k" is the wave number [18].

II.3. *Computation of Radiation Pattern of Rectangular Acoustic Aperture*

Although the circular radiating aperture is a classic example of an acoustic transducer, an open-ended rectangular aperture shown in Fig. 8 is the most widely used acoustic radiating aperture element. As in circular radiating aperture, the rectangular aperture also consists of infinitesimally small point sources with dimension "ds" at distance "ρ" from the center of the aperture. The expression for the radiation patterns of a rectangular aperture is given by:

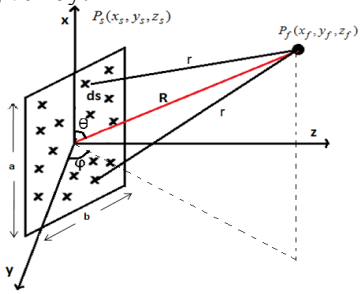

Fig. 8. Coordinate system of rectangular aperture for analysis radiation pattern

$$P_f(x_f, y_f, z_f) = \iint_{surface} P_s\, ds$$

$$= A_0 \frac{e^{-jkr}}{r} \int_{x=-a/2}^{a/2} \int_{y=-b/2}^{b/2} e^{j(k[x.\sin\theta.\cos\varphi + y.\sin\theta.\sin\varphi])}\, dx\, dy \quad (3)$$

$$= A_0 \frac{e^{-jkr}}{r} \int_{x=-a/2}^{a/2} e^{j(kx[x.\sin\theta.\cos\varphi])}\, dx \int_{y=-b/2}^{b/2} e^{j(ky[\sin\theta.\sin\varphi])}\, dy \quad (4)$$

Where, $\theta = 0\ to\ a$
$\varphi = 0\ to\ 2\pi$

In Eq. 4, "P_s" indicates pressure field of a point source on rectangular aperture, $a \times b$ arethe length and height of the rectangular aperture, "r" is distance between the observation point "P_f" and the point source "P_s", "R" is a distance of observation measured between the observation point and the center of rectangular aperture and "k" is the wave number. A conventional circular and rectangular aperture with the associated coordinate system for the analysis of near field radiation pattern is shown in Fig. 9. The radiating aperture of the circular and rectangular transducer is assumed to coincide with Z=0 plane or XY plane. The observation point "P_f" is in the near-field range of the transducer.

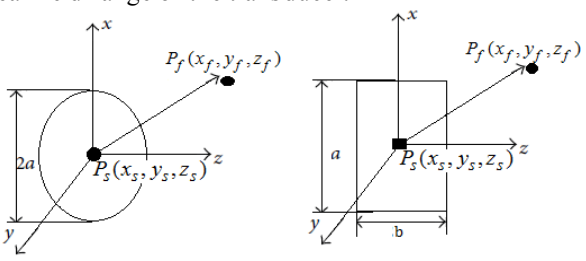

(a) (b)

Fig. 9. Coordinates of observation point and radiating point source

The Cartesian coordinates of the observation point "P_f" are given by:

$$x_f = R \sin\theta_f \cos\varphi_f \quad (5)$$
$$y_f = R \sin\theta_f \sin\varphi_f \quad (6)$$
$$z_f = R \cos\theta_f \quad (7)$$
$$r = \sqrt{(x_f - x_s)^2 + (y_f - y_s)^2 + (z_f - z_s)^2} \quad (8)$$

Where, $\theta_f = -90^0\ to + 90^0$
$\varphi_f = 0\ to\ 360^0$

(x_s, y_s, z_s) and (x_f, y_f, z_f) denote the coordinates of a point sourceand the observation point respectively. The functional relationship between the positional coordinates of field point $(r, \theta, \varphi, x_f, y_f, z_f)$, the variables (x, y, z) and pressure field distribution at point sources on circular and rectangular aperture are explicit in Eqs. (5) to (8) and Fig. 9 [19]. It is relevant to emphasize that the formulation presented in this paper is valid for any distance of observation from the acoustic transducer.

III. Results and Discussion

This section presents a discussion on the simulation results of radiation patterns of circular and rectangular acoustic apertures obtained through the formulations presented in the earlier sections. The results include the surface contour plots of pressure distribution over the radiating aperture, near and far-field radiation patterns of both the circular and rectangular apertures. The discussion in this section also covers the validation studies of far-field results obtained through the proposed near-field analysis of acoustic transducer. For the simulation, the chosen operating frequency for both the apertures is 30 kHz which is well within the SONAR operating frequency range of 10 kHz to 300 kHz, [20].

Fig. 9(a) shows the geometrical configuration of an acoustic transducer with a circular aperture. For an acoustic transducer of circular aperture with a radius of (rad = 2cm; D= 4cm), at a frequency of 30 kHz (λ = 4.9cm, c = 1480 m/s). The near-field distance has to be less than $2D^2/\lambda$ (<6.54cm). When the radial distance of observation is $R > 2D^2/\lambda$, it satisfies the far field distance criterion. Fig. 9(b) illustrates a geometrical configuration of a transducer with a rectangular aperture of length a = 2.89cm and

height b = 4.34cm. For excitation of point source points on the acoustic aperture, 36 x 36 point sources along the radial (ρ), as well as azimuthal (φ) directions on the aperture, are considered on the radiating apertures of both the circular and rectangular configurations. The pressure field distributions over circular and rectangular apertures are shown in Fig. 10 (a) & (b) respectively through contour image.

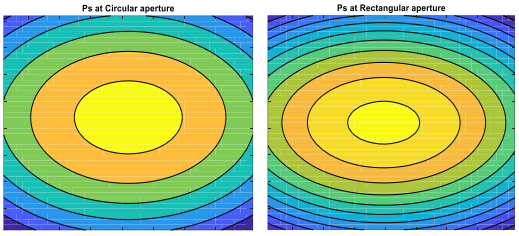

(a) (b)

Fig. 10. Pressure distribution over (a) circular and (b) rectangular aperture

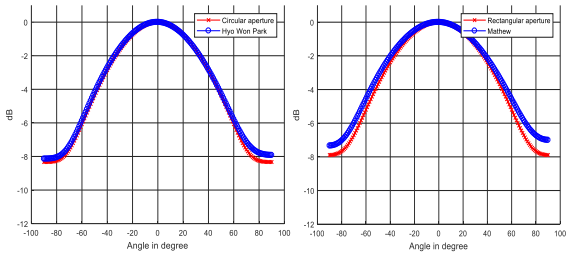

(a) (b)

Fig. 11. Comparison of far-field radiation patterns of (a) proposed circular aperture with [7]; (b) proposed rectangular aperture with [21]

Fig. 11 illustrates the comparison of the results obtained from the far-field analysis of existing methods and the far-field as a special case of the near-field analysis proposed in this paper. Fig. 11(a) shows the comparison of the far-field radiation pattern of circular aperture obtained from the proposed analysis and the results of the method proposed in [7]. Similarly, Fig. 11(b) shows the comparison of results of the far-field radiation pattern of acoustic rectangular aperture obtained through the proposed analysis and the results through the analysis in [21]. The results of Fig. 11 show the excellent correlation between the proposed near-field/far-field method and existing the far-field techniques. The results of Fig.11 also show that the main beam of the circular and rectangular aperture is almost identical. This is because the area of circular and rectangular apertures is chosen to be the same for the simulation studies. It is pertinent to emphasize that the formulations presented in [7] and [21] are applicable only for far-field analysis and not valid for near-field analysis.

After validating the simulated results on far-field radiation patterns of circular and rectangular apertures, the computations of near-field radiation (amplitude and phase) patterns were carried out using the proposed analysis with the radial observation distance of R= 0.8 D^2/λ (where, "R" is the range, "D" is the dimension of the transducer and "λ" is the wavelength of acoustic waves) at a frequency of 30 kHz for an illustration of a comparison of radiation patterns at near-field and far-field regions. Fig. 12(a) shows the comparison of the NF ($R=0.8D^2/\lambda$) and FF ($R=2D^2/\lambda$) amplitude patterns of a circular aperture. The corresponding results for a rectangular aperture are shown in Fig. 12(b). Fig. 13(a) shows the phase patterns of circular aperture at ($R=0.8D^2/\lambda$) and FF ($R=2D^2/\lambda$). The corresponding results fora rectangular aperture are shown in Fig. 13(b).

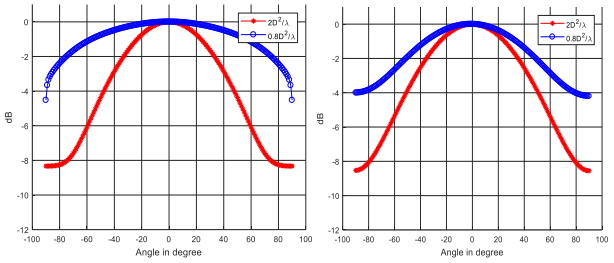

(a) (b)

Fig. 12. Comparison of amplitude radiation patterns of (a) circular aperture and (b) rectangular aperture

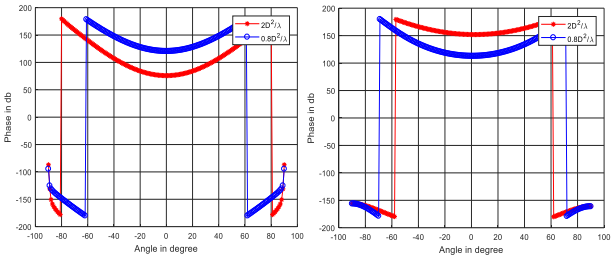

(a) (b)

Fig. 13. Phase radiation patterns of (a) circular aperture and (b) rectangular aperture

The analysis of near field radiation pattern is carried out with an incremental increase in the radial distance of observation. Simulations were carried out to obtain the near-field patterns of circular and rectangular apertures at distances of $0.2*D^2/\lambda$, $0.4*D^2/\lambda$, $0.6*D^2/\lambda$, $0.8*D^2/\lambda$, $1.2*D^2/\lambda$, $1.6*D^2/\lambda$, $2*D^2/\lambda$, $4*D^2/\lambda$. Figs. 14 and 15 show the radiation patterns of circular aperture and rectangular apertures for the above mentioned radial distances of observation respectively. Simulation results indicate that, when the distance between the observation point and the aperture is small, no formation or no clear formation of the main beam is evident. As the distance between the aperture and observation point increases, the progression in the formation of the main beam is clearly seen.

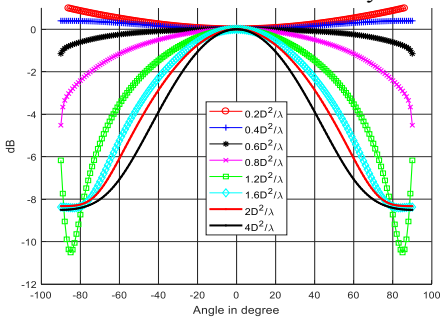

Fig. 14. Radiation pattern of circular aperture for different radial distance

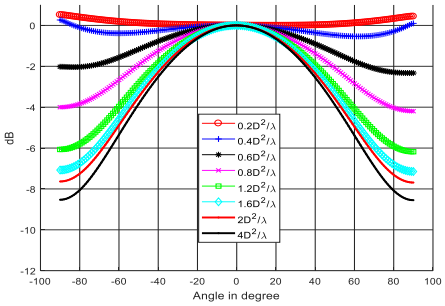

Fig. 15. Radiation pattern of rectangular aperture for different radial distance

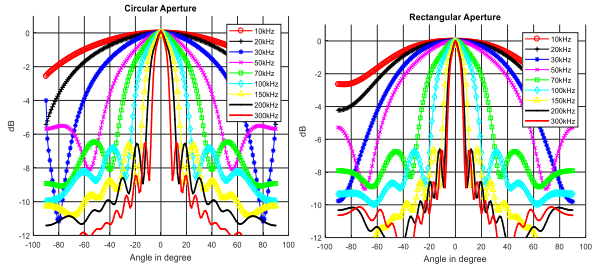

(a) (b)

Fig. 16. Comparison of radiation pattern of (a) circular and (b) rectangular aperture for different frequencies (10 kHz to 300 kHz) when range "R = D^2/λ" is varying

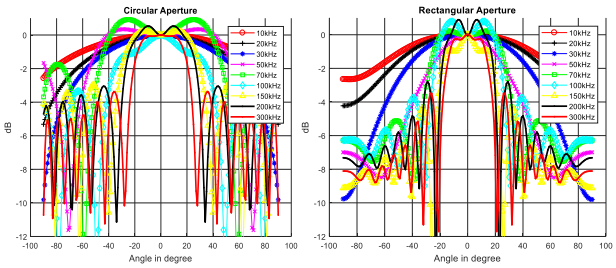

(a) (b)

Fig. 17. Comparison of radiation pattern of (a) circular and (b) rectangular aperture for different frequencies (10 kHz to 300 kHz) when range "R = 0.0324cm" is fixed

Figs. 16 &17 show the near-field radiation pattern of circular and rectangular apertures. Figs. 16(a) & (b) illustrate the radiation pattern of circular and rectangular aperture for different frequencies from low to high (10 kHz to 300 kHz) with R = D^2/λ. However the absolute value of "R" varies since "λ" also changes with frequency. Figs. 17(a) & (b) illustrate the radiation pattern of circular and rectangular aperture for different frequencies from low to high (10 kHz to 300 kHz) when range "R" is fixed to near-field region (R = D^2/λ at frequency f = 30 kHz; R = 0.0324cm). The results of Figs. 17 (a) and (b), reveal that as the frequency increases, profile of the radiation patterns shows lot more rapid variations (fluctuations).

IV. Conclusions

This section summarizes the conclusions derived which are based on the analysis and simulation results presented in this paper. The proposed formulation for computing the radiation pattern of the acoustic transducer is valid for both the near-field and far-field regions. With the prior knowledge of pressure distribution on the radiating aperture, the proposed near-field analysis is valid for a wide variety of acoustic transducer geometries. The radiation pattern of the acoustic transducer at any arbitrary point of observation (both the near-field and far-field) is obtained by the vector summation of the fields radiated by the array of point sources located on the aperture of the acoustic transducer. The validity of the proposed approach for computing the radiation pattern of the acoustic transducer is substantiated by correlating the obtained the far field results with those obtained through existing far field techniques. Unlike the proposed analysis, the other existing techniques [7] and [21] are meant only for the far field radiation pattern and they do not apply to the near field scenario. The simulation studies show that the near field radiation patterns of the acoustic transducer exhibit changes in the profile of the amplitude patterns when the distance of observation is varied. The formation of the well-defined main beam occurs only after a distance of separation from the radiating aperture (R=1.2D^2/λ).The presented analytical formulation has an attribute of wider generality given its applicability to a variety of geometrical configurations of the aperture of the acoustic transducer. The analytical formulation for the radiation pattern of acoustic transducer which valid for an arbitrary distance of observation will be significant relevance to near-field beamforming array, which is a topic of current interest of the authors.

References

[1] Khairul A. Ahmad, A.B.D. Manaf, M.F.A. Rahman, Design of polyimide based piezoelectric micro-machined ultrasonic transducer for underwater imaging application, *Proceedings of the International Conference on Imaging, Signal Processing and Communication*, pp. 63-66, Penang, Malaysia, 2017.

[2] G. Suresh, V. Natarajan, A. Shanavas, Underwater imaging using acoustic lens, *IEEE Underwater Technology, Chennai, India, 2015*

[3] Zaiqing Meng, *A Study on a synthetic aperture sonar*, Ph. D Thesis, Loughborough University of Technology, UK, 1995.

[4] W. K. Blake, T. D. Le, and J. R. Peoples, Target interpretation using inverse synthetic aperture sonar techniques, *The Journal of the Acoustical Society of America, Vol. 90, issue 4,1998*

[5] Nadim M. Daher and Jesse T. Yen, 2-D array for 3-D ultrasound imaging using synthetic aperture techniques, *IEEE Transactions on Ultrasonics, Ferroelectrics, and Frequency Control, Volume: 53*, (Issue 5), *pages. 912-924, 2006.*

[6] J. George and Vinod Kumar, A Review of advances in synthetic aperture sonar imaging algorithms, *International Journal of Innovative Research in Electrical, Electronics, Instrumentation and Control Eng., Vol. 3, 2016.*

[7] Hyo Won Park, *Modeling and Simulation of Acoustic Pressure Field for Ultrasonic Tactile Displays*, Master thesis, Lehigh University, Pennsylvania, USA, 2017.

[8] C. Q. Qu, Research on signal of field monitor of 7220a localizer beacon subsystem of ILS, *Open Journal of antennas and Propagation, pp. 37-50, 2015.*

[9] A. R. Selfridge, G. S. Kino and B. T. Khuri-Yakub, A theory for the radiation of a narrow-strip acoustic transducer, *Journal for Applied Physics Letters, Volume 37,* (Issue-1), *1980, pages 35-36.*

[10]Rongrong Lu, Rama Rao and Nafi Toksoz, *Measured radiation patterns of the scale model dipole tool*, Master of Science Thesis.

Massachusetts Institute of Technology, Cambridge, MA, 2014.
[11]Hayden J. Callow, *Signal processing for synthetic aperture sonar image enhancement*, Ph.D. Thesis. University of Canterbury, Christchurch, New Zealand, 2003.
[12]Peter R. Stepanishen, Transient radiation from pistons in an infinite planar baffle, *The Journal of the Acoustical Society of America, vol. 49, 2005, pages 1629-1971.*
[13]Haim Azhari, *Basics of biomedical ultrasounds for engineers*, 1st Edition, (John Wiley and sons, 2010, pp. 153-185).
[14]Alan J. Hunter, *Underwater acoustic modelling for synthetic aperture sonar*, Ph.D. thesis, University of Canterbury, Christchurch, New Zealand, 2006.
[15]Constantine A. Balanis (1997), *Antenna Theory: Analysis and Design*, (©John wiley & Sons, Inc., 1997, pp. 25-105).
[16]Martin Trusler, *Physical acoustics and metrology of fluids*, (© Tylor and Francis Group, LLC, 1991, pp. 116-178).
[17]Whitlow W. L. Au, Mardi C. Hastings, *Principles of Marine Bioacoustics*, (© Springer Science+Business Media, LLC, 2008, pp. 27-117).
[18]F. G. Mitri, Partial-wave series expansions in spherical coordinates for the acoustic field of vortex beams generated from a finite circular aperture, *IEEE Ultrasonics, Ferroelectrics, and Frequency Control Society, Volume 61,* (Issue 12), *2014, pages 2089 – 2097.*
[19]Fridolin P. Mechel, *Formulas of Acoustics*, (© Springer-Verlag Berlin Heidelberg, New York, 2008, pp. 74-269).
[20]O. Oralkan, A. S. Ergun, C. H. Cheng, J.A. Johnson, M. Karaman, B.T. Khuri-Yakub, Underwater acoustic imaging using capacitive micro-machined ultrasonic transducer arrays, *IEEE conference on OCEANS '02MTS, 2002, pages 2354-2360.*
[21]Jasmine Mathew, *Acoustic Radiation and Scattering from Cylindrical Bodies and Analysis of Transducer Arrays*. Ph.D. thesis. Naval Physical and Oceanographic Laboratory, DRDO 2011.

Authors' information

[1]**Praveen L. S.** works as an Assistant Professor at M. S. Ramaiah University of Applied Sciences, Peenya, Bangalore-560058**.** Author completed BE in Medical Electronics, Visvesvaraya Technological University, Karnataka. M. Sc. [Engg.] in Signal Processing and Communication Engineering and pursuing Ph.D. in Imaging SONAR

[2]**Govind R. Kadambi** works as an Pro-vice chancellor at M. S. Ramaiah University of Applied Sciences, Peenya, Bangalore-560058**.** Author completed BE in Electronics and Communication Engineering in University of Mysore. M. S. in Antenna, IIT, Madras and Ph. D. in Antenna, IIT, Madras.

[3]**S. Malathi** works as an Associate Professor at M. S. Ramaiah University of Applied Sciences, Peenya, Bangalore-560058**.** Author completed B.E in Electronics and Communication Engineering, Madras, University, 1996. M.E in Microwave and Optical Engineering, Madurai Kamaraj University, 1999 and Ph.D. Indian Institute of Science, Bangalore, 2012.

[4]**Preetham Shankapal works** as an Data Scientist in GE Healthcare, Bangalore-560058**.** Author completed B.E in Medical Electronics Visvesvaraya Technological University, Karnataka. M. Sc. [Engg.] in Biomedical Engineering in University of Warwick and Ph.D. in Imaging RADAR, Coventry University.

